Fractals, Vol. 26, No. 5 (2018) 1850067 (10 pages)

DOI: 10.1142/S0218348X18500676

World Scientific
www.worldscientific.com

FRACTAL DIMENSION DETERMINATION OF ROCK PORES BY MULTI-SCALE ANALYSIS OF IMAGES OBTAINED USING OM, SEM AND XCT

ISMELI ALFONSO* and ALBERTO BELTRÁN
Instituto de Investigaciones en Materiales, Unidad Morelia
Universidad Nacional Autónoma de México
Campus Morelia UNAM, Antigua Carretera a Pátzcuaro
No. 8701, Col. Ex-Hacienda de San José de la Huerta
C. P. 58190, Morelia, Michoacán, México
**ialfonso@unam.mx*

MOHAMED ABATAL and IVÁN CASTRO
Facultad de Ingeniería, Universidad Autónoma del Carmen
Campus III, Avenida Central S/N, Esq. con Fracc. Mundo Maya
C. P. 24115, Ciudad del Carmen, Campeche, México

ALEJANDRA FUENTES, LEONOR VÁZQUEZ and ARMANDO GARCÍA
Tecnología Aplicada en Exploración y Producción Petrolera
S. A. de C.V. (TEMPLE), Calle 33 Num. 145 2do, Piso Depto.
"F". Col. Burócratas, C. P. 24160, Cd. del Carmen, Campeche, México

Received December 5, 2017
Accepted May 7, 2018
Published October 2, 2018

Abstract

The present work includes the analysis of the porosity at different scales using image characterization techniques. Porosities were determined and compared for reservoir rocks through the fractal dimensions obtained from two-dimensional (2D) image analysis. Studies were developed

*Corresponding author.

using Optical Microscopy (OM), Scanning Electron Microscopy (SEM) and X-ray Computed Tomography (XCT). In order to compare the images and analyze the similarities in the porosities, the box-counting method was used to extract the power-law distributions and to obtain the fractal dimensions. Results showed that fractal dimensions were similar for the three different techniques, which included different scale analysis, fact that demonstrates the fractal character of the porosity in the studied systems. The effectiveness of the use of 2D image analysis and the importance of the multiscale study of the porosity were also demonstrated.

Keywords: Fractal; Rock; Pore; SEM; Tomography.

1. INTRODUCTION

Extraction processes for oil, natural gas or geothermal fields are highly dependent of the reservoir characteristics, mainly the permeability (k). Most permeability assessments are carried out on cores extracted from the reservoir, inferred from pressure and flow rate data, as the works of Glover *et al.*[1] or Farrell *et al.*[2] k has been calculated from porosity (ϕ) measurements using different models.[3–5] These relationships between k and ϕ motivate the use of image processing, from micro or macrographies obtained using different techniques and at different scales, to analyze the pore systems in rocks. Among these techniques are thin section Optical Microscopy (OM), Scanning Electron Microscopy (SEM) and X-ray Computed Tomography (XCT), as observed in the work of Hemes *et al.*[6] One of the most important disadvantages related to the use of images obtained using OM or SEM is due to sample preparation. For example, Loucks *et al.*[7] reported that pore system is not readily observable by conventional sample-preparation methods due to the fact that most pores are difficult to differentiate from sample-preparation artifacts, mainly for small nanometric pores. Besides, the sample has to be cut and cannot be used anymore afterwards. XCT overcomes these limitations because almost no sample preparation is needed for equipment with large sample chambers, being a reference method for porosity evaluation. This technique captures the true topology of the porous system because the internal structure of the sample remains unchanged. Assuming that the XCT image resolution is sufficient to capture the realistic pore network, these studies can provide the basis for generating three-dimensional (3D) models. However, a major limitation of the XCT, besides the high cost, is the inability to resolve small features, as shown in the work of Best,[8] necessarily the complementation with other techniques, e.g. SEM (although now synchrotron tomography can reach spatial resolutions down to 50 nm). The study of small pores can be included into models of dual porosity, incorporating microporosity into a physically representative macro-pore network, as obtained by Best,[8] dividing the total pore space into macro-porosity (pores $> 2\,\mu$m) and micro-porosity (any pore space $< 2\,\mu$m). A similar dual porosity analysis using OM and SEM digital image analysis over more than three orders of magnitude was studied by Anselmetti *et al.*,[9] classifying the pores into macro-pores ($>500\,\mu\text{m}^2$) and micropores ($<500\,\mu\text{m}^2$). These authors also established the equation for determining the total porosity as follows:

$$\Phi_{\text{tot}} = \Phi_{\text{mac}} + \Phi_{\text{mic}}(1 - \Phi_{\text{mac}}), \tag{1}$$

where Φ_{tot}, Φ_{mac} and Φ_{mic} are total, macro- and micro-porosities, respectively.

From the analysis of the above-mentioned works, it can be seen that some studies dispute the use of SEM due to problems originated by sample preparation, scanning position, magnification, etc., while other works use SEM information in the study of small pores. Different division limits into micro- and macro-porosity are also established. We think that the study of the fractal characteristics of pore systems could help in the analysis of the effectiveness of SEM for the study of the micro-porosity, in which the used division limit is not significant. Although papers discussing the methodology of fractal analysis of fracture patterns are widely available,[10,11] fractal study of the matrix porosity is understudied. The porosity (ϕ) is mainly coupled with the pore size distribution and with the fractal dimension (D_f), according to[4,5]

$$\phi = \left(\frac{r_{\min}}{r_{\max}}\right)^{d_E - D_f}, \tag{2}$$

where $r_{\min}$ and $r_{\max}$ are the minimum and maximum pore radii, and d_E is the Euclidian dimension.

Besides, the pore morphology and pore-size distribution show scaling behaviors characterized by D_f, and its estimation should not depend upon the technique involved in its determination, and probably upon the scale of investigation, as demonstrated by Kruhl[12] and Hemes *et al.*[6] Then, if D_f determined using SEM and XCT at different scales were similar, two points could be shown: (1) the fractal character of the specific porous system in the studied scale range, i.e. similarity in pore distributions, and (2) the effectiveness of SEM for the study of a porous system as a complementary method for different scales characterization. The most common method to determine D_f is image analysis, obtaining the structure of a porous medium and quantifying the self-similarity or the fractal dimension of the structure. D_f is mainly determined using the box-counting method, where the object (set of pores in this case) is covered with an unsteady lattice of unit grid of size l, and the number of non-empty boxes is determined.[13] Mathematics of this method is relatively easy, the box-counting dimension being one of the mostly used ones. The fractal property characterized by D_f using box-counting method is obtained from

$$D_f = \lim_{\delta - 0} \log N(\delta) / \log \delta, \tag{3}$$

where δ is the magnification factor or scale (corresponding to the inverse of the grid size l) and $N(\delta)$ is the number of self-similar parts under the fixed magnification factor. For the analysis, a two-dimensional (2D) binary object with size $N \times N$ is used, in this case corresponding to the pore–rock matrix binary image. Then, the probability of a pore to be counted into a box is analyzed, and the quantity of porous spaces with a determined size is plotted. The accuracy of D_f determination depends not only on the sample preparation and the characterization technique, but also on the image analysis method. Different methods and software quantify microstructures by image processing, as used by Liu *et al.*,[14] based on the identification of isolated regions in a binary image. The key issue of the technology is how to segment the image, so that determined pixels represent pores in the binary image. Nevertheless, these reported comparisons do not include direct analysis of images obtained using 2D and 3D methods. The complete 3D structure can be obtained using XCT by measuring the 2D X-ray attenuation at a series of angles as the object is rotated. That is why 2D individual images are obtained, which are projected to generate the 3D file. Then, the XCT 2D images can be compared to 2D images obtained by using other characterization techniques, being adequate for validation purposes.

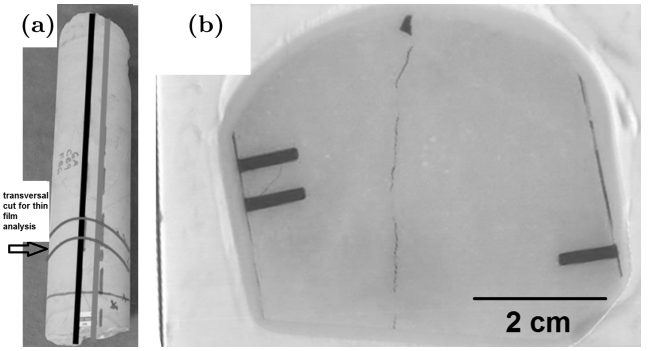

Fig. 1 Macrographies of the **(a)** core extracted from the Chiapas zone, and **(b)** thin section obtained from the thick zone, marked in the core.

Based on the above analysis, this paper has two goals: (1) to probe the fractal character of a specific porous system in the studied scale range, and (2) to validate the effectiveness of 2D microscopy of thin sections for the study of a porous system. Keeping these purposes in mind, the porosity of different reservoir rocks was studied using three techniques: OM and SEM of thin sections, and XCT of core plugs. The combination of these techniques allowed the analysis of the porosity at three different scales for pore sizes ranging between 0.1 μm and 20 mm. The fractal dimension was the parameter used for comparison purposes, analyzing the effect of the scale and the characterization techniques on it.

2. EXPERIMENTAL

2.1. Sample Preparation and Image Capture

For this study, samples were collected from nine wells from the Sierra de Chiapas region, Mexico, located in a range between 300 and 2500 m above sea level (ASL). The analyses of the samples included XCT, OM and SEM. Sample preparation procedures were focused on the needs of each technique. For XCT analysis, samples were 5 cm in diameter and 20–30 cm in height cylinders from drill cores collected from depths between 0.5 and 32 m. These samples were analyzed using a General Electric HiSpeed QX/I helicoidal scanner with a voltage of 140 kV, current 150 mA and a time of 2 s.

Figure 1a shows a typical drill core used for the analyses, in this case from the well with the code P1. For microscopy analysis, thick sections (10–15 mm in thickness) were obtained from the cores and injected with blue epoxy, as can be observed in Fig. 1a. From these samples, thin sections were obtained and grinded using a 1 μm Al_2O_3 grit. Figure 1b shows a typical thin film obtained from the extracted cores. As pores are filled with blue epoxy, therefore, for the OM analysis, the blue areas are recognized as connected pore space; while for SEM analysis, image mode provides excellent signal to noise even at a low voltage, necessary for the study of non-conductive samples without metal coating. Due to the resin filling the pores, they are darker than the matrix. A petrographic Olympus BX53 OM, in transmission mode, was used for the study of thin sections, also analyzed by using a Hitachi S-3400N Variable Pressure SEM, operated at 10 kV and 30 Pa using the Backscatter Electron compositional mode. For microscopy studies, two thin sections were analyzed for each plug. Ten images were obtained for each thin section from different zones for a better statistical analysis.

2.2. Image Processing

The pore system captured in the images was analyzed through the pixels intensity, which can be converted to area or length, depending on the characterization method. The true equivalent pore diameter can be then calculated from the pixel/real scales ratio of the images, which is 10 pixels/μm for SEM images, 1.10 pixels/mm for OM images and 3.85 pixels/mm for XCT images. The maximum box size used in each case corresponded to the maximum size of the observed pores, which helps to separate the observation scales and to limit micro- and macro-porosities. First, the obtained gray-level images were transformed to binary ones. Due to the insertion of the colored epoxy resin into the porous media, for SEM images, the porosity is clearly distinguished, being darker than the matrix. An effective segmentation method used to analyze the pores in these images is the global thresholding method, described in the work of Liu *et al.*,[14] in which the gray-level image is converted into a binary one by selecting an appropriate gray-level threshold in order to separate the pores from the background.[15] ImageJ software was used for image analysis and D_f determination.[16] Taking into account pixels/length ratios, D_f were determined using Eq. (1) by the box-counting method. The δ versus $N(\delta)$ log–log graphs were modified using the size in μm instead of pixels to show the different scales used. For comparison purposes, the null hypothesis that the standard deviations for D_f obtained using the different techniques are the same was established.

3. RESULTS AND DISCUSSION

As already discussed, the scales used for the analyses were different. The resolution range included pores from 0.1 μm (SEM images) to 20 mm (XCT). Although 2D XCT micrographs were obtained from three different planes, as observed in Fig. 2a, the analyses were developed using only the transversal Z plane micrographs (see Fig. 2b). These Z planes were used because thin films were also obtained by cutting cross-sections. An example is observed in Fig. 2c, which shows an SEM image obtained from a thin film. This technique was used for the study of the pores of lower size, being much more important to complement the results obtained at higher scales.

Figures 3a and 3b show micrographies obtained using XCT and SEM, respectively, and processed using ImageJ, highlighting the importance of these

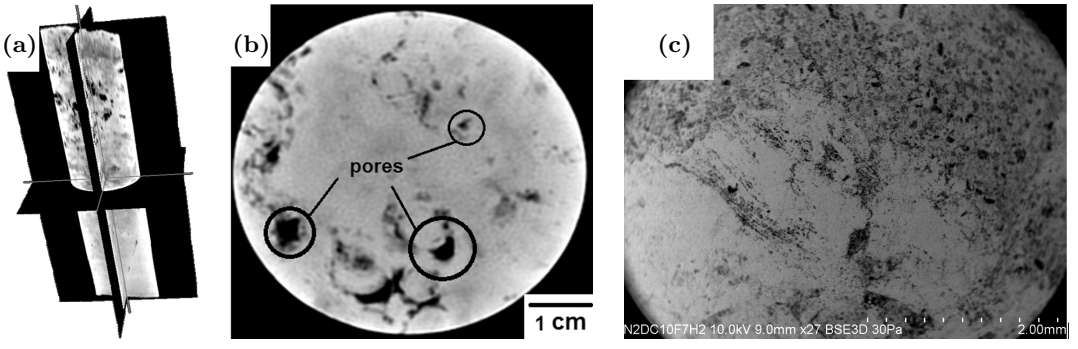

Fig. 2 XCT images of the **(a)** longitudinal X and Y planes, and **(b)** transversal Z plane of the cores. **(c)** SEM image for the thin film of a selected zone. Porosity can be observed (dark zones).

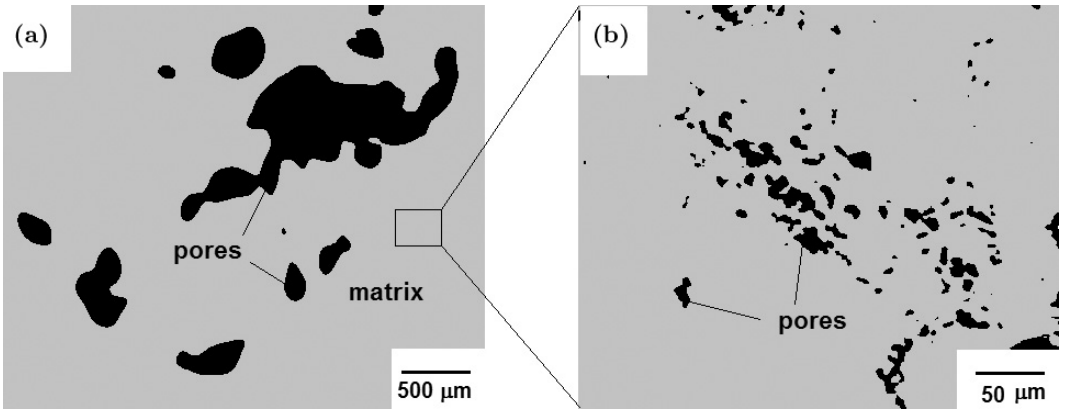

Fig. 3 Processed micrographies showing the total porosity separated into macro-pores and micro-pores, obtained, respectively, using **(a)** XCT and **(b)** SEM.

complementary techniques to study the two kinds of porosities. Figure 3a shows the macro-porosity (in black) and the matrix, where a rectangular area was maximized through SEM analysis to demonstrate the presence of micro-porosity in the matrix (see Fig. 3b). Due to the size of these small pores, they cannot be observed using OM, or the XCT used in this work, because pores are smaller than the resolution limit of the equipment. The use of SEM allows to complement these techniques when no expensive XCTs are available.

Once the images were obtained using the three analysis techniques, fractal dimension was determined for each case and compared at different scales in a log–log graph. To show the analyses used here, three study cases are shown in this work, corresponding to three different wells: P2 (2400 m ASL), P3 (859 m ASL), and P4 (1110 m ASL). It is

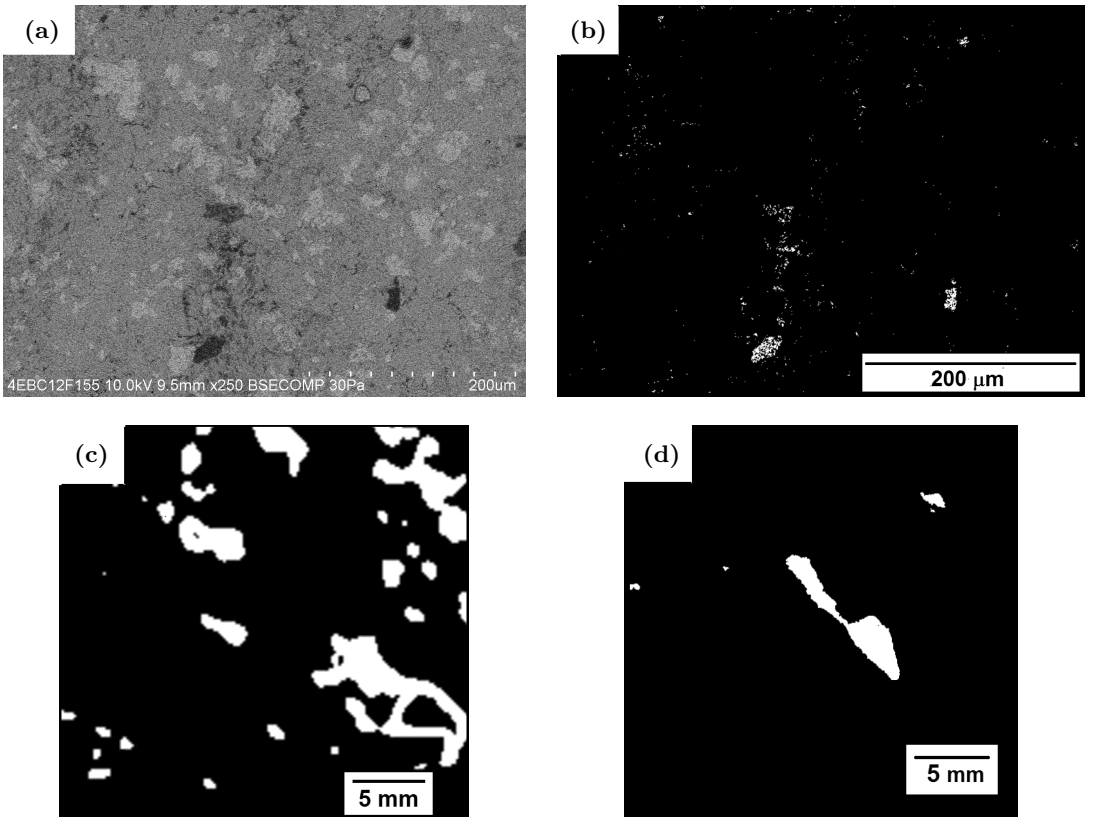

Fig. 4 **(a)** SEM image for a selected zone of the thin film, for the well P2; and **(b)** the same image (threshold binary) processed using ImageJ. **(c)** XCT and **(d)** OM binary images, processed using ImageJ.

important to remark that this work does not analyze the effect of the depth of the sample in the well, but only similarities for the pore network at different scales for the same sample. Figures 4a–4d show the analysis for the cores obtained from the well P2. Figure 4a shows that the micro-porosity for this sample is low, reaching an average volume fraction of 0.0568. The image processed using ImageJ can be observed in Fig. 4b, showing the pores in white to have a better background. For these particular images, at ×250, 1 pixel = 0.4 μm. Otherwise, Figs. 4c and 4d show the processed images obtained using XCT and OM, respectively. For XCT images, the analyzed pores are in the range between 260 and 20,000 μm, and 1 pixel = 260 μm, while for OM images, 1 pixel = 91 μm, the pores being in the range between 91 and 12,000 μm. Porosity measured using XCT was 0.054. Total porosity calculated using Eq. (1) was 0.108.

The comparison between the average fractal dimensions obtained using the three techniques, for the sample P2, can be observed in Fig. 5. As mentioned above, the box size was measured in μm scale instead of pixels to show the different scales used (remember that the maximum box size used in each case corresponded to the maximum size of the pores). The log–log graph contains the information of the images obtained from each technique. This graph was divided into three sections: (i) SEM section, for pore sizes between 0.4 and 100 μm; (ii) OM section, for pore sizes higher than 90 μm; and (iii) XCT section, for pore sizes higher than 260 μm. As can be observed, OM and XCT sections overlap beyond 260 μm. Lines obtained using these

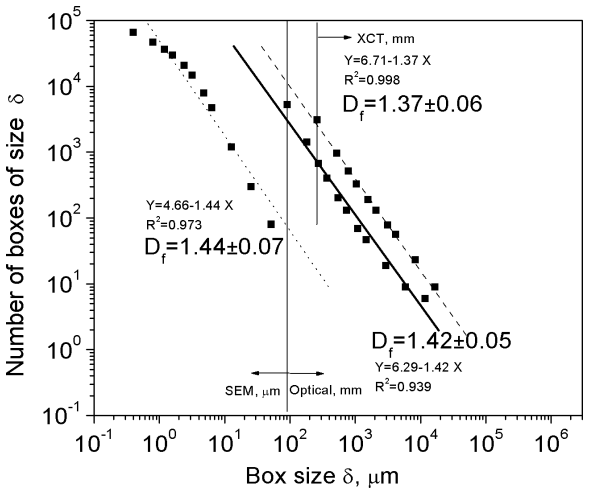

Fig. 5 Fractal dimensions for different scales for the sample P2.

two techniques include pores at the same scale and should be very close, in which the main difference is not in the X-axis but in Y-axis (the total quantity of measured pores). Then, the limit for pore classification into micro- and macro-pores could be established in ∼90 μm. This classification is more approximated to the established one by Anselmetti *et al.*,[9] because our limit (90 μm) corresponds to ∼2000 μm,[2] quite different from the one reported by Best[8] (only 2 μm). If the XCT or OM used in our work had higher magnifications, this limit could be lower. An important conclusion derived from these analyses is that the study of the porosity could include micro/macro pore limits depending on the available characterization techniques, not predetermined. This figure also shows that the correlation coefficients are high, an indication of the validity of the calculated fractal dimensions. On the basics of the null hypothesis and the analysis of the standard deviations, D_f shows no significant differences, the lines being parallel between them at different scales. These results show the fractal character of the porosity for this rock sample, being self-similar in the analyzed scales. Fractal theory establishes that a geometry is fractal if it presents low quantity of features (e.g. pores) of big size, increasing exponentially the quantity of these features of smaller sizes, and this relation being invariable within certain scales.[16] Then, and according to the work of Mandelbrot,[17] the behavior of the porosity at each scale in our work can be defined as self-similar fractal due to the log–log plots depicting continuous lines, far different from a standard Euclidian form, where a constant horizontal line is obtained. A small deviation of the slope can be observed for the case of smaller pores, where the behavior could be still cataloged as self-similar, even far different from the non-ideal fractal behavior reported by Rigaut,[18] where two asymptotes could be defined (including an Euclidian part). This small deviation for the smaller pores in Fig. 5 could be originated by the resolution limit of the image, close to the size of these pores. Several works use surface area adjustments for obtaining only one slope.[18–20] In our work, by comparing the average correlation value (D_f) for each scale (obtaining three parallel lines), we are avoiding the problems originated by measurable quantities depending on the scale. The similitude between the D_f values obtained using this method demonstrates its efficacy. According to Pape *et al.*,[19] fractals are characterized by their property to be structured to infinity

in the same way, due to the theory of fractal dimensions belonging to mathematics. Nevertheless, real objects may show a fractal behavior over a large range, as observed for porous rocks. So, petrophysical investigations make sense of the range of scales studied in our work, and smaller pores could be also studied and maybe defined into a fractal or non-ideal fractal. The study of sizes over approximately six orders of magnitude (from 10^{-1} to $10^{5}\,\mu$m), and the suggested scale-invariance, opens the possibility of up-scaling our observations to larger scale characteristics of the porous space.

In order to corroborate the results for well P2, other wells were analyzed. Figures 6a–6d show the analysis for the cores obtained from the well P3. Figures 6a, 6b and 6c show the images treated by ImageJ, obtained from SEM, XCT and OM analysis, respectively. For this sample, the microporosity was higher than that for the P2 well, reaching an average volume fraction of 0.144 (measured using SEM images), and 0.158 measured using XCT. In this case, total porosity was 0.279. The comparison between the average fractal dimensions obtained using the three techniques can be observed in Fig. 6d. In this case, the high correlation coefficients also indicate the validity of the calculated fractal dimensions. For these samples, the analysis of the D_f values also shows no significant differences, the lines being parallel between them. In this case, the lines obtained using OM and XCT are very close, fact originated by the similarities in the total quantity of pores measured for each technique, not observed in Fig. 5. A small deviation of the slope is also observed for the pores analyzed by using SEM, but in this case, it is lower than that for Fig. 5. These results corroborate the fractal character of the porosity, being self-similar in the analyzed scales. It is important to remark, and according to Eq. (2), that porosity is not only affected by D_f, but also by the differences between minimum and maximum pore sizes, fact that could explain that although D_f are similar for P2 and P3, the porosity for P3 is higher (smaller differences between minimum and maximum pore radii).

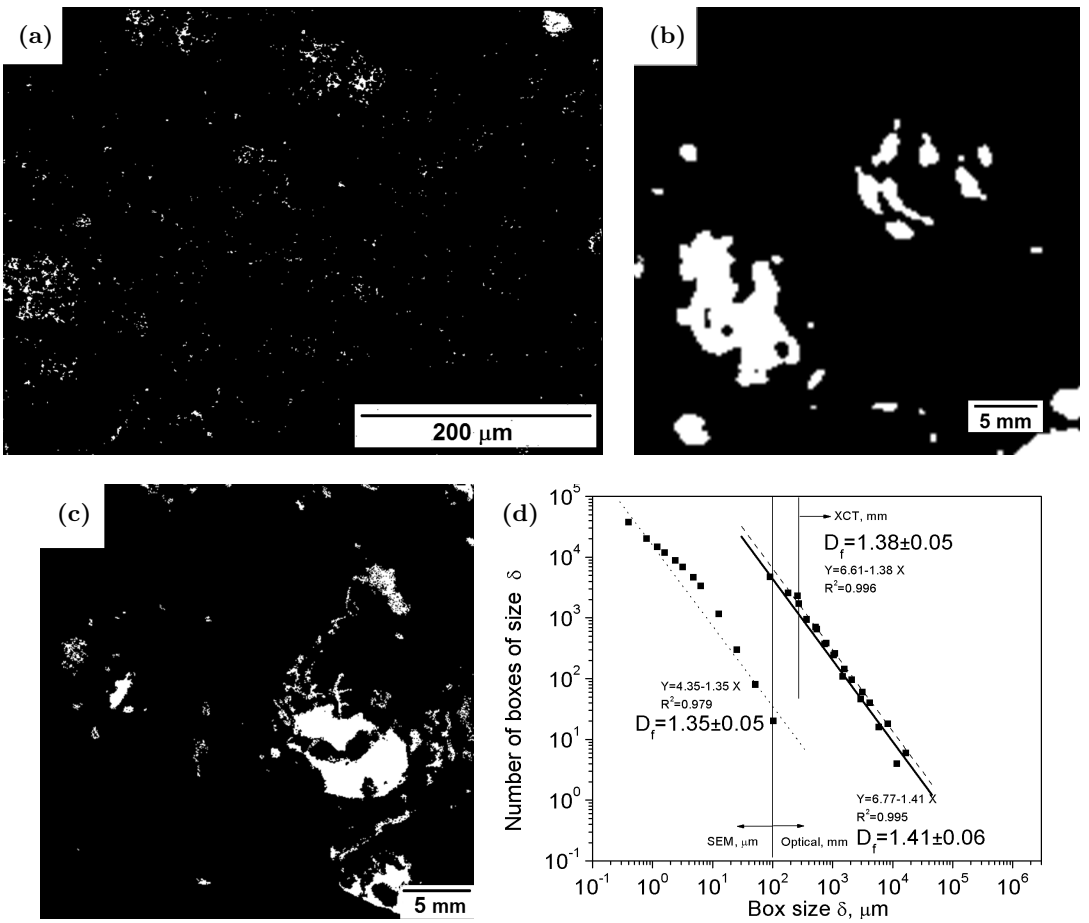

Fig. 6 ImageJ processed images (threshold binary), for the well P3, obtained using **(a)** SEM, **(b)** XCT and **(c)** OM analysis. **(d)** Fractal dimensions for different scales.

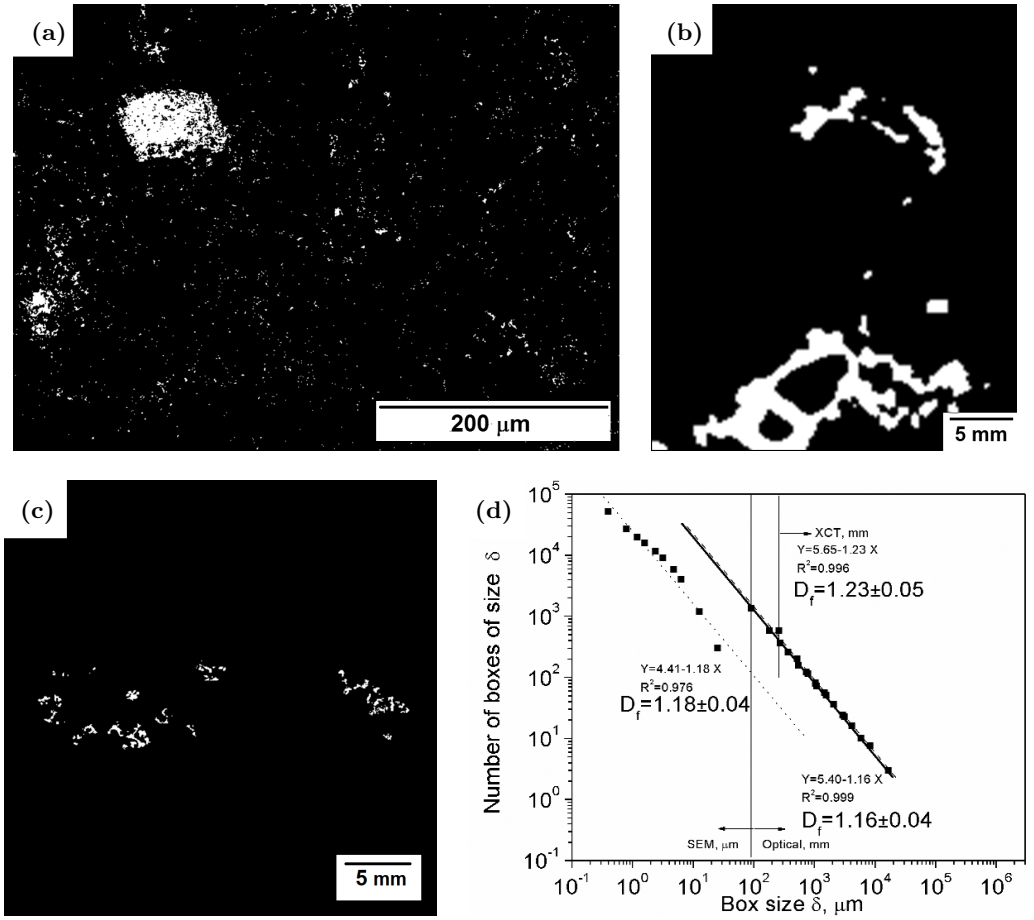

Fig. 7 ImageJ processed images (threshold binary), for the well P4, obtained using **(a)** SEM, **(b)** XCT and **(c)** OM analysis. **(d)** Fractal dimensions for different scales.

A third study case can be observed in Figs. 7a–7d, for the well P4. For this sample, micro-porosity volume fraction was 0.117 (using SEM), while macro-porosity was 0.066 (using XCT), also showing no significant differences between the values of D_f, the lines being parallel between them. In this case, total porosity was 0.231. These results demonstrate the fractal character of the rock for this sample; and the similarities of the pore networks at different scales (the aim of the present work). The small deviation of the slope for the smaller pores is also observed in this case.

In Conclusion, after the analysis of these three samples, fractal dimensions agree for the different techniques. This result was repetitive for other wells of the Chiapas region, not presented in this work. These analyses will be very useful in finding a correlation between micro-porosity and permeability in rocks, derived from the similitude between micro- and macro-porosities, and will be analyzed in future works. Besides, other fluid/rock interactions could be better understood, as established by Anovitz and Cole,[20] who mentioned the importance of the multiscale quantification techniques, being possible to correlate the statistical analysis of relatively large rock volumes with images of the pores themselves; or Xu *et al.*,[21] who presented a fractal dual-porosity model which helps to a better understanding of fluid transport physics of fractured porous media. It is important to remark that although a fractal study can describe the scaling behavior of porous systems, it is not sufficient to fully quantify the pore structure.[6] The reason for this is that it does not fully describe how a fractal structure fills space, in our case corresponding to the texture of the pore structure. To address this limitation, two additional parameters could be introduced in future works: (i) the lacunarity or gappiness; and (ii) the succolarity or connectivity of the pore structure.

4. CONCLUSION

After the analysis of the porosity for different samples of rocks, using three different image techniques

at different magnification scales, and their comparative fractal study, it can be concluded as follows:

(1) The fractal dimensions neither depend on the scale studied nor on the used technique, demonstrating the scale-invariance and self-similarity of the porosity in the studied scale range.
(2) The effectiveness of 2D image characterization techniques was demonstrated and, obtained by using the preparation techniques described in the present work, for the study of the porosity in these rock systems.
(3) The use of standard preparation techniques for thin films also demonstrated to be adequate for the study of the micro-porosity in these materials using SEM.
(4) The presence of two kind of porosities was demonstrated, and divided in micro- and macro-pores. The limits between these pores really depended on the available characterization techniques.
(5) The characterization methodology presented in this work for the study of the porosity at different levels could be extended to the characterization of different porous systems.

ACKNOWLEDGMENTS

The authors would like to acknowledge the financial support from CONACYT–SENER 143927 for funding the project. The support from TEMPLE (Tecnología Aplicada en Exploración y Producción Petrolera SA de CV) is also acknowledged. Authors would also like to acknowledge Guillermo C. Aguilar Palma for his technical support.

REFERENCES

1. P. W. J. Glover, I. I. Zadjali and K. A. Frew, Permeability prediction from MICP and NMR data using an electrokinetic approach, *Geophysics* **71**(4) (2006) F49–F60.
2. N. J. C. Farrell, D. Healy and C. W. Taylor, Anisotropy of permeability in faulted porous sandstones, *J. Struct. Geol.* **63** (2014) 50–67.
3. D. Benavente, C. Pla, N. Cueto, S. Galvañ, J. Martínez-Martínez, M. A. García-del-Cura and S. Ordóñez, Predicting water permeability in sedimentary rocks from capillary imbibition and pore structure, *Eng. Geol.* **95** (2015) 301–311.
4. P. Xu, H. Liu, A. P. Sasmito, S. Qiu and C. Li, Effective permeability of fractured porous media with fractal dual-porosity model, *Fractals* **25**(4) (2017) 1740014.
5. P. Xu, A discussion on fractal models for transport physics of porous media, *Fractals* **23**(3) (2015) 1530001.
6. S. Hemes, G. Desbois, J. L. Urai, B. Schröppel and J. O. Schwarz, Multi-scale characterization of porosity in Boom Clay (HADES-level, Mol, Belgium) using a combination of X-ray μ-CT, 2D BIB-SEM and FIB-SEM tomography, *Micropor. Mesopor. Mat.* **208** (2015) 1–20.
7. R. G. Loucks, R. M. Reed, S. C. Ruppel and D. M. Jarvie, Morphology, genesis, and distribution of nanometer-scale pores in siliceous mudstones of the Mississippian Barnett shale, *J. Sediment. Res.* **79** (2009) 848–861.
8. S. Best, Development and implementation of a dual-porosity pore network structure using X-ray computed tomography for pore network modeling purposes, thesis, Master of Science in Civil Engineering, Louisiana State University, US (2011).
9. F. S. Anselmetti, S. Luthi and G. P. Eberli, Quantitative characterization of carbonate pore systems by digital image analysis, *AAPG Bull.* **82**(10) (1998) 1815–1836.
10. J. J. Walsh and J. Watterson, Fractal analysis of fracture patterns using the standard box-counting technique: Valid and invalid methodologies, *J. Struct. Geol.* **15** (1993) 1509–1512.
11. Q. Zhu, W. Yang and H. Yu, Study on the permeability of red sandstone via image enhancement, *Fractals* **25**(6) (2017) 1750055.
12. J. H. Kruhl, Fractal-geometry techniques in the quantification of complex rock structures: A special view on scaling regimes, inhomogeneity and anisotropy, *J. Struct. Geol.* **46** (2013) 2–21.
13. T. Tel, A. Fulop and T. Vicsek, Determination of fractal dimensions for geometrical multifractals, *Physica A* **159** (1989) 155–166.
14. C. Liu, B. Shi, J. Zhou and C. Tang, Quantification and characterization of microporosity by image processing, geometric measurement and statistical methods: Application on SEM images of clay materials, *Appl. Clay Sci.* **54** (2011) 97–106.
15. R. Stoessel, T. Guenther, T. Dierig, K. Schladitz, M. Godehardt, P. M. Kessling and T. Fuchs, μ-computed tomography for micro-structure characterization of carbon fiber reinforced plastic (CFRP), in *QNDE 2010*, San Diego, pp. 461–468.
16. W. S. Rasband, ImageJ, U. S. National Institutes of Health, Bethesda, Maryland, USA (1997–2018), https://imagej.nih.gov/ij/.
17. B. B. Mandelbrot, *Fractals*: *Form*, *Chance and Dimension* (Freeman, San Francisco, 1977).
18. J. P. Rigaut, An empirical formulation relating boundary lengths to resolution in specimens showing

'non-ideally fractal' dimensions, *J. Microsc.* **133** (1984) 41–54.
19. H. Pape, L. Riepe and J. R. Schopper, Theory of self-similar network structures in sedimentary and igneous rocks and their investigation with microscopical and physical methods, *J. Microsc.* **148** (1987) 121–147.
20. L. M. Anovitz and D. R. Cole, Characterization and analysis of porosity and pore structures, *Rev. Mineral. Geochem.* **80** (2015) 61–164.
21. P. Xu, C. Li, S. Qiu and A. P. Sasmito, A fractal network model for fractured porous media, *Fractals* **24**(2) (2016) 1650018.